Uncertainty Maps for Seismic Images through Geostatistical Model Randomization

Lewis Li and Jef Caers, Department of Energy Resources Engineering, Stanford University;
Paul Sava, Department of Geophysics, Colorado School of Mines

Summary

Much of the difficulties in characterizing complex reservoirs are related to the uncertainty associated with seismic interpretation. In this project, we examine two such sources: uncertainty in the velocity model, and ambiguities with expert interpretation due to conceptual geological uncertainty of reservoir structure. We address the first issue by presenting a geostatistical method for generating multiple velocity models to capture this uncertainty. We take this a step further by obtaining a set of migrated images using these multiple models, and build uncertainty maps based on local Euclidean and Procrustes distances between the migrated images. These uncertainty maps can aid an interpreter in deciding a) if certain structures actually are present in the image and b) the spatial placement of existing structures. An illustration to subsalt imaging is provided.

Introduction

While advancements of seismic imaging have provided reservoir modelers with improved input for reservoir characterization, there are still large uncertainties associated with the seismic imaging itself and with the interpretations made on such images. One cause of uncertainty is due to the use of uncertain velocity models, which in turn leads to uncertain depth migration. Furthermore, due to the computational burden of migration and time spent on interpretation, generally only a single image is processed and interpreted. Common practice is to then stochastically perturb faults and horizon locations to capture uncertainty (Thore et al. 2002). However, this type of analysis neglects the uncertainty in the seismic velocity itself, as well as the uncertainties associated with both manual and automatic interpretation (Suzuki et al, 2005).

While there exists a wide variety of commercial automatic interpretation tools, the majority of them rely on tracking of amplitude peaks that are not applicable for complex reservoirs, and manual structural interpretation by an expert remains the status quo. Unfortunately, the images may be of limited resolution, and/or poor quality, making this a difficult task. An example is given by Bond et al (2008) who obtained interpretations from 412 experts on the same synthetic seismic image, of which only 21% correctly identified the correct tectonic setting. They suggested the need for tools to help minimize the effects of such 'conceptual uncertainty'. For instance, consider the seismic image of a target reservoir zone shown in Figure 1. Upon initial examination, one may interpret this to contain faults, and perhaps submarine canyons. In actuality, this seismic image was obtained via migration using an imperfect salt velocity model and with patchy illumination. Had perfect

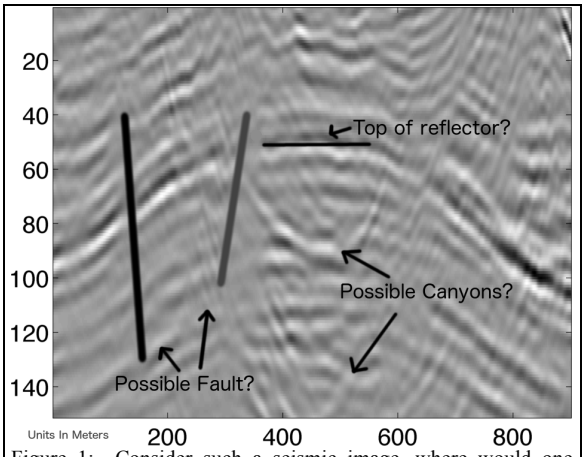

Figure 1: Consider such a seismic image, where would one interpret the reflectors, faults and canyons to be? Where is the top of the main reflector?

velocity and acquisition been used, then the seismic image would appear as shown in Figure 2. We note that there are neither canyons nor faults, in this region, and the artifacts that appear in Figure 1, arise due to our limited understanding of the velocity model. Furthermore, we note that the vertical position of the main reflector is also shifted.

This mimics a scenario common in reality; the best estimate of the velocity model is imperfect, and as a result the migrated image exhibits artifacts that may appear as real structures (a common problem in the case of Bond et al., 2008), and improperly positioned layers. The question we attempt to address is, how starting with a single velocity model can we identify regions of high uncertainty, thus aiding the expert during interpretation? To address the issue of uncertainty in the velocity model, attempts have been made to generate multiple velocity models, and thus multiple images. Clapp (2003) presents a methodology through which a prediction error filter and 1-D Dix inversions are used to generate velocity realizations. While this method showed promise, it was applicable only on smoothly varying 1-D velocity profiles. In this project, we developed a novel fractal based geostatistical simulation that can generate multiple realizations of 2D or 3D velocity models containing complex subsurface structures such as salt bodies. Using these velocity realizations and their

correspondingly migrated images, we construct uncertainty maps by means of image analysis techniques to identify regions where artifacts may occur, and locations where structure positioning may be uncertain.

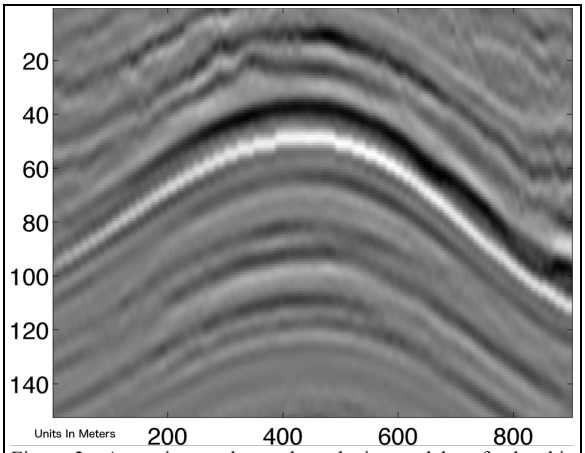

Figure 2: Assuming we knew the velocity model perfectly, this is the seismic image we expect to see. Note that there are neither canyons nor faults. Furthermore, the top of the main reflector is higher than it appears to be in Figure 1.

Geostatistical Randomization of Model Parameters

While a variety of model parameters are used in seismic migration, we focus our attention on the velocity model. Consider the scenario, where the best estimate for a velocity model containing a complex salt body is given in Figure 3. Salt's high seismic wave velocity causes it to act as a lens during imaging, and thus uncertainties in the salt structure have significant effects on the resulting image. Consequently, we generate new velocity models in which the salt boundaries shift in position, while retaining the overall characteristics of its shape. The workflow is outlined in Figure 4.

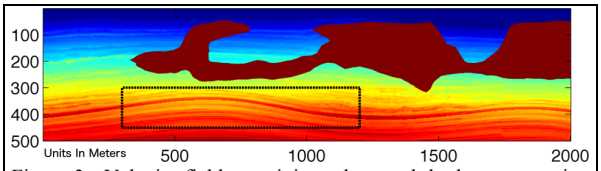

Figure 3: Velocity field containing a large salt body, representing the best estimate of the velocity model. A geostatistical randomization is applied to generate new realizations with varying boundary positions while retaining the overall characteristics of the body. The target reservoir zone is indicated by the dashed box.

Identify Salt Body

The first step is to identify the shape and location of the salt body in the reference velocity model, for example as

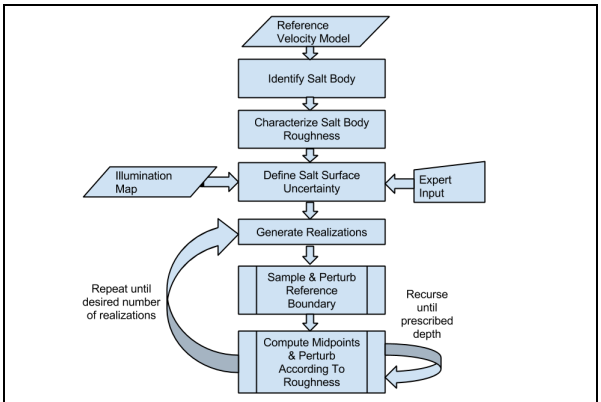

Figure 4: Workflow of fractal-based simulation of salt body realizations.

obtained from standard seismic processing. This can be accomplished using an edge detection filter followed by a boundary-tracing algorithm to produce a contour of the salt body. Alternative techniques could include Hough (Duda, 1972) or Radon transforms (Deans, 2007).

Characterizing Salt Body Roughness

We note that the salt body's geometric shape displays fractal properties. Fractals as introduced by Mandelbrot (1967), have long been used in a geological context. They are defined as sets that display self-similarity; that is they appear the same at every scale. One property is that fractals can be characterized by its *fractal dimension* can be used for characterization. Mathematically speaking, the fractal dimension is a statistical measure of the complexity as a ratio of the change in detail to the change in scale. There is no single definition of the fractal dimension; but we use the Minkowski-Bouligand dimension (Kenneth, 1990) for the purpose of this study. It states that for a given set S, and N($\boldsymbol{\varepsilon}$) is the number of boxes with side length $\boldsymbol{\varepsilon}$ required to cover the set, the dimension is given as:

$$\dim(S) = \lim_{\varepsilon \to 0} \frac{\log N(\varepsilon)}{\log 1/\varepsilon} \qquad (1)$$

The fractal dimension is thus a single parameter that is not necessarily an integer, which describes a fractal shape. It should also be noted that the fractal dimension is a not a unique descriptor and lacks the necessary information to perfectly reconstruct the shape. It can however, be used to describe physical attributes such as roughness (Pfiefer, 1984). Consequently, we can parameterize the salt boundary as fractal dimension, and then use it later to generate new boundaries with the same dimension/attributes.

Defining Salt Surface Uncertainty

Before geostatistical generation of salt body realization can proceed, we need to specify the local uncertainty around the salt body surface. In regions of high uncertainty,

realizations of the salt boundary surface need to fluctuate more, while the contrary applies to regions with low uncertainty. One method of selecting an uncertainty buffer would be for an expert to define this based on his/her intuition. Alternatively, illumination can be used as a metric to automatically construct such uncertainty model, which we term the "uncertainty buffer". For instance, in Figure 5, illumination has been shown with the original salt body overlaid. Accordingly, regions with low illumination (blue) will result in wide uncertainty buffers, while high illumination (red) will yield narrow buffers.

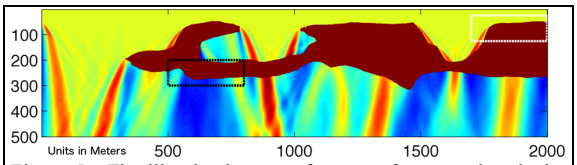

Figure 5: The illumination map for our reference salt velocity model. This is used to generate uncertainity buffers for our salt body

Generating Realizations

Generation of the realizations can be accomplished by: sampling points along the boundary from the original salt body, perturbing it by a noise scaled by the size of the local uncertainty buffer, and interpolating between these sampled points using a fractal algorithm. For two-dimensional cases such as this, the midpoint displacement algorithm can be used, while in three dimensions, the diamond-square algorithm can be applied (Miller, 1986). The midpoint displacement algorithm works by computing the midpoint between sampled points, and then perturbing it by some noise. This process is recursively applied with the perturbation noise decreasing at each level proportional to the fractal dimension. This is repeated until a prescribed recursive depth is achieved. The resulting set of points represents the boundary of the salt body in the new realization. The points can be connected to generate a continuous boundary. The resulting realization will resemble the original velocity model in terms of roughness, but the boundaries will be more varied in regions of low illumination, and less varied in regions of high illumination. Figure 6 depicts regions from sample realizations exhibiting this behavior.

Distance Based Generation of an Uncertainty Map

Having generated a set of velocity realizations, we can then proceed with performing migration, yielding a set of seismic images. While it would be ideal for an expert to interpret all resulting migrations, we recognize that this is generally not feasible. Instead, we aim to develop a single uncertainty map from this set of images and provide it as an interpretation tool that highlights areas of the seismic image that are most uncertain.

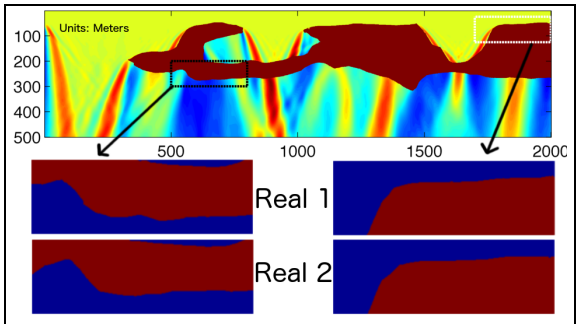

Figure 6: Regions from sample realizations generated from the reference velocity model in Figure 3, and uncertainity buffers defined using the illumination map shown in Figure 5. Note that regions of low illumination exhibit more variation, while regions of high illumination exhibit little variation between realizations.

We can identify regions of high uncertainty within the image by examining which areas vary the most across the entire set of images. In other words, areas of low uncertainty should appear to be similar in every image. Therefore, by taking a window around each voxel in the reference image, and comparing it to the same window over all other images, we can produce an uncertainty map that gives a voxel wise model of uncertainty. The question is therefore on the nature of the distance/metric used to compare the images.

Euclidean Distance:

A simple metric would be the average difference between corresponding pixels across the set of images. For the sake of illustration, we constructed 100 salt body realizations using the aforementioned fractal methodology. Twelve representative realizations were selected using the methodology outlined in Scheidt and Caers (2009), and migrated. We then computed an uncertainty map using the Euclidean distance in a region of the image centered on the target zone illustrated in Figure 1. Figure 6 shows the uncertainty map overlaid with the image generated using the reference velocity (Figure 3). Examining the migrated images, it can be seen that the reflectors shift vertically, with the greatest variation in the middle. This explains why the uncertainty map indicates the greatest uncertainty in that particular region. This concurs with the observation made by examining the reference image with the truth; that the center of the reflector are more uncertain that the sides.

Procrustes Distance:

The Euclidean image only looks at voxel-wise comparison and may not reflect properly variation in patterns (sets of voxels) between images. For this reason we investigate the use of the Procrustes distance, a statistical shape analysis that is used to measure similarity of shapes (Hurley & Cattell, 1962).

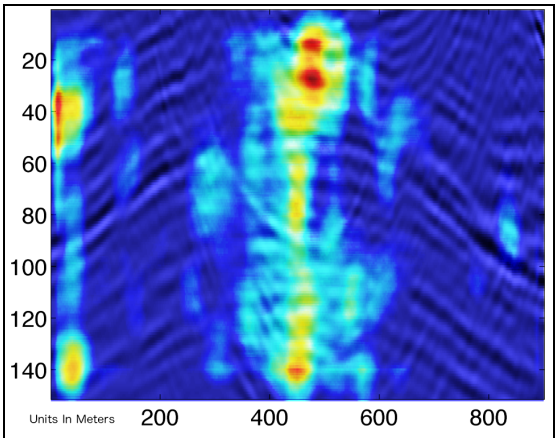

Figure 6: Uncertainity map generated using Euclidean distance on our set of migrated images.

Given two shapes with points at coordinates (x_{j1}, y_{j1}, z_{j1}) and (x_{j2}, y_{j2}, z_{j2}), the algorithm proceeds in four steps:

1. Compute centroid of each shape, and compute translation between the two:

$$(\bar{x}, \bar{y}, \bar{z}) = \left(\frac{1}{n} \sum_{j=1}^{n} x_j , \sum_{j=1}^{n} y_j , \sum_{j=1}^{n} z_j \right) \quad (2)$$

2. Use Frobenius norm as shape size metric to compute scale change required:

$$S(x) = \sqrt{\sum_{j=1}^{n} [(x_j - \bar{x})^2 + (y_j - \bar{y})^2 + (z_j - \bar{z})^2]} \quad (3)$$

3. Compute optimal rotation to superimpose the two shapes. If $\mathbf{x}_1$ and $\mathbf{x}_2$ are *n* x *3* matrices containing shape coordinates, we apply a SVD to $\mathbf{x}_1^T \mathbf{x}_2$ to obtain $\mathbf{UDV}^T$, the rotation matrix is then given by $\mathbf{VU}^T$.
4. We apply the transformations computed in previous three steps. The Procrustes distance is defined as the sum of squared point distances after transformation

$$P_d^2 = \sum_{j=1}^{n} [(x_{j1} - x_{j2})^2 (y_{j1} - y_{j2})^2 + (z_{j1} - z_{j2})^2)] \quad (4)$$

In our application, we pre-process the images by applying an edge filter; creating a binary image highlighting the major reflectors. When Procrustes analysis is performed, the distance is now a measure of the shape variation of reflectors and structures amongst the set of images. For instance, while the middle of the reflectors in the generated realizations vary in vertical location, their shapes are similar, and Procrutus analysis indicates a low distance in those areas. Conversely, Figure 7 shows that the regions of high uncertainty are now aligned with the vertically dipping reflectors/canyons. This is an indication that in these regions, the shapes of the structures vary across the set of realizations, which is in line with the fact that such structures are artifacts resulting from an inaccurate velocity model. The Procrustes-based uncertainty map allows identifying with uncertainty in reflection patterns resulting in uncertainty in geological structure, including the locations of possible artifacts.

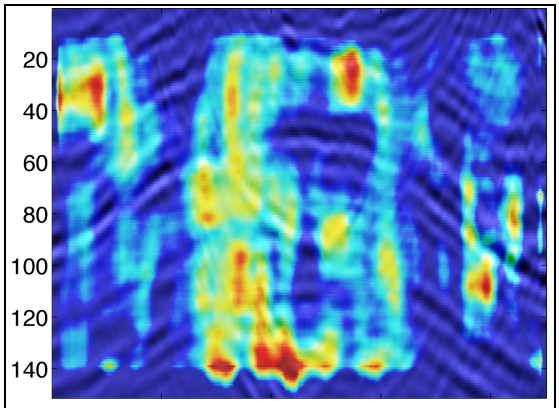

Figure 7: Uncertainity map generated using Procrustus distance on our set of migrated images.

Conclusion

In this study, we investigate two sources of uncertainty associated with seismic characterization. The first, arising from uncertainty in the velocity model, can be addressed by generating multiple velocity realizations. We developed a fractal-based geostatistical method for generating realizations by varying lithologic boundaries. The second cause of uncertainty lies in the interpretation of seismic images. To this end, we generated multiple velocity models, and invoked different measures of distances on the migrated images to generate various uncertainty maps. It was found that a Euclidean-distance-based uncertainty map was able to capture spatial uncertainty of structures, while a Procrutes map was able to indicate regions of structural uncertainty. We conclude that the two maps are complementary, and when used together can aid an expert in interpretation by providing insight into various kinds of image uncertainty. Such measures could perhaps also be used for automatic interpretation tools.

Acknowledgements

The authors would like to thank the SCRF (Stanford Center For Reservoir Forecasting) affiliates and CWP (Center For Wave Phenomena) sponsors for their support. We would also like to extend our gratitude to SEG for providing the SEAM model used here for illustration.